BULLETIN OF THE EARTHQUAKE
RESEARCH INSTITUTE
Vol. 48 (1970), pp. 87-114

7. *Free Oscillations of the Earth Excited by the Kurile Islands Earthquake 1963.*

By Katsuyuki ABE, Yasuo SATÔ,
Earthquake Research Institute.
and Jose FREZ,
International Institute of Seismology and Earthquake Engineering.

(Read September 22, 1969.—Received January 21, 1970.)

Abstract

Power spectrum data are obtained from the free oscillations of the earth excited by the Kurile Islands earthquake of October 13, 1963, and recorded at eleven stations of WWSSN. Eigen periods of fundamental free oscillations are determined for spheroidal modes 7 to 50, and torsional modes 7 to 46. Equivalent phase velocities are also calculated from the observed periods over the period range from 820 to 170 sec. Observed periods differ slightly from one station to another, and such divergence becomes significant for periods shorter than 350 sec. This difference in the observed period may suggest that the relative amplitudes of the individual modes are affected by a lateral heterogeneity of the upper mantle not deeper than several hundred kilometers.

From the amplitude decay with time, the attenuation of free oscillations is estimated for a number of spectral peaks. For the spheroidal oscillation, the average Q factor is 251 for $n=13-17$ ($T=380-480$ sec), and 200 for $n=18-42$ ($T=200-380$ sec).

Various studies are made on the spectral amplitudes to obtain the source-space function of the earthquake and the pattern of free oscillation modes on the sphere. The results are almost consistent with the earthquake mechanism and mode excitation as revealed by other studies, though the pattern of oscillation is hard to recognize.

1. Introduction

The measurement of free oscillations of the earth provides a lot of information concerning the earth's interior. The low order free oscillations are affected by the density distribution in the lower mantle and the core, while high order oscillations are closely connected with the shear velocity distribution in the upper mantle. Numerous analyses have been carried out by many authors. Those works have been reviewed by *Bolt* [1964], *Press* [1964], *Anderson* [1965], and *Smith* [1967]. A recent review by *Anderson* [1967] contains a list of available data of eigen

periods. The amplitude of spectral peaks also contains useful information concerning the anelastic property of the earth [*Ness et al.*, 1961]. The amplitude and phase provide useful knowledge of the source parameters such as source dimension, rupture velocity, and mechanisms of the earthquake [*Benioff et al.*, 1961; *Press et al.*, 1961; *Smith* 1961].

In order to investigate the subjects stated above, we analyzed the seismograms of the Kurile Islands earthquake of October 13, 1963. The USCGS determination of the epicenter is 44.8°N, 149.5°E, and the origin time is 05h 17m 57.1 sec (GMT). The magnitude is 7 3/4-8 by Palisades and 8 1/4 by Pasadena. The mode analysis of free oscillations of this earthquake has been carried out by *Alsop* [1964a] and *Dziewonski* and *Landisman* [1969]. The following analyses and discussions are given in the present paper:

(1) Eigen periods and equivalent phase velocities for both spheroidal and torsional oscillations.

(2) Quality factor Q of spheroidal oscillations.

(3) Amplitude of spectral peaks and the determination of the azimuthal order number m for spheroidal oscillations.

(4) Expansion of the amplitudes corrected for Q, into spherical surface harmonics.

(5) Phase angles of free oscillations observed at various stations.

2. Data and method of analysis

Full size copies of Press-Ewing long period seismograph records from eleven stations of WWSSN were used for the analysis. The response of these instruments was almost identical. Figure 1 shows the response curve calculated with Hagiwara's formula assuming $\sigma^2=0.2$, which is a plausible value as a coupling factor that expresses the reaction of the galvanometer [*Hagiwara*, 1958].

The records were traced and digitized with a uniform sampling rate by an electronic curve reader and were automatically punched in 5 digit numbers. The accuracy of the sampling rate was checked by comparing the total length of record with the number of data points. The digitized data were plotted and checked against the original records. The short period waves with periods less than about 40 sec were carefully smoothed by eye before digitizing. A constant shift and linear trend were removed. Then, the 3-point and 5-point smoothings were consecutively performed, and one out of every three points was adopted to reduce the number of data points. With this operation no aliasing is caused. The power transfer ratio of the numerical filter is shown in Fig. 2.

After these operations, we used the method of spectrum analysis as described by *Blackman* and *Tukey* [1958] except for the phase analysis,

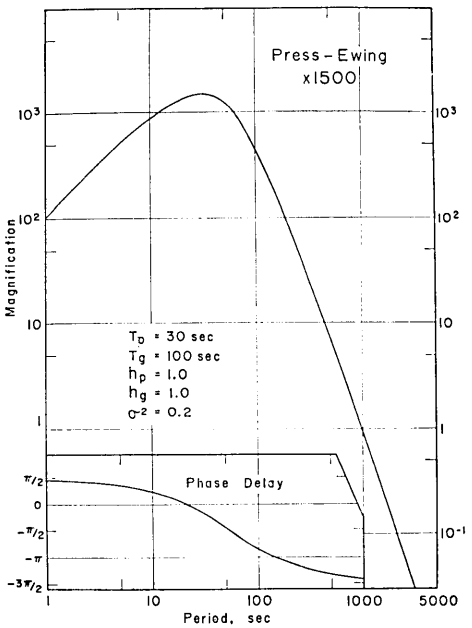

Fig. 1. Instrument constants, magnification, and phase delay of the Press-Ewing seismograph used in the analysis. The constants T_p and h_p are natural period and damping constant of the pendulum, while T_g and h_g are those of the galvanometer. σ is the coupling factor.

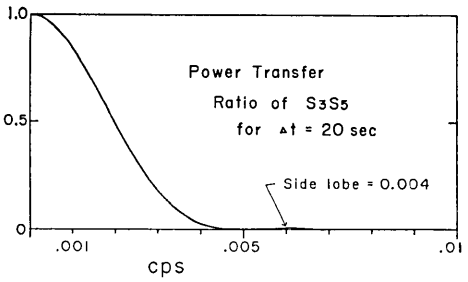

Fig. 2. The power transfer ratio of the digital filter used to eliminate high-frequency wave from the digitized data.

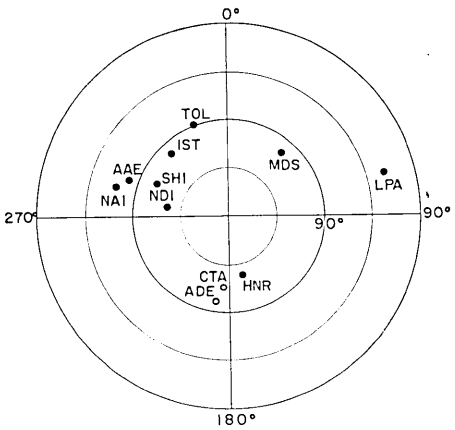

Fig. 3. Geographic distribution of eleven WWSS stations used in the present study. The filled and open circles indicate the stations used for the analysis of spheroidal and torsional oscillations respectively. The center indicates the epicenter, and the station location is plotted by polar coordinate.

where we used direct Fourier analysis. The auto-correlation was taken for the individual record, and then the cosine transform was performed with the fast Fourier transform program [*Cooley* and *Tukey*, 1965]. Finally refined spectral densities were estimated by using the hanning window. Of the eleven WWSSN records, nine vertical components at SHI, IST, NAI, HNR, NDI, MDS, TOL, LPA and AAE were analyzed for the spheroidal oscillation, and two horizontal ones at CTA and ADE for torsional oscillations. The locations of stations and sampling time intervals are listed in Table 1 together with other data (also see Fig. 3). The azimuth of great circle path from the epicenter to the station is measured clockwise from the north as seen in the table.

The calculated power spectral densities at each station are presented in logarithmic scale in Figs. 4*a*, *b*, *c*, *d*, *e*, *f*. In these power spectra,

Table 1. List of stations and data used in power spectrum analysis.

Kurile Islands: Date 13 Oct. 1963, origin time 05:17:57.1, Depth 60 km, Lat. 44.8°N, Long. 149.5°E

Station	Component	Latitude (deg)	Longitude (deg)	Distance (deg)	Azimuth* (deg)	Initial Point(GMT)	Record Length(hour)	Digital Spacing(sec)
						h m s		
SHI	V	29.8N	52.9E	74.0	296.1	09 05 00	15.5	20.40
IST	V	41.0N	29.0E	79.3	318.5	08 42 00	19.3	20.92
NAI	V	1.3S	36.8E	106.9	285.5	08 50 40	19.8	20.44
HNR	V	9.4S	160.0E	54.8	167.4	08 48 04	20.3	20.39
NDI	V	28.7N	77.2E	58.3	280.3	08 44 04	15.8	20.40
MDS	V	43.4N	89.8W	77.6	39.9	09 20 00	13.2	20.44
TOL	V	39.9N	4.0W	92.4	339.9	09 05 01	14.3	20.43
LPA	V	34.9S	57.9W	156.8	74.3	08 29 58	14.0	20.41
AAE	V	9.0N	38.8E	98.0	291.1	08 40 58	16.0	20.41
CTA	EW	20.1S	146.3E	64.6	183.4	09 12 02	14.7	20.44
ADE	EW	35.0S	138.7E	80.0	189.0	08 00 00	13.6	20.37

* Azimuth at epicenter, measured clockwise from the north.

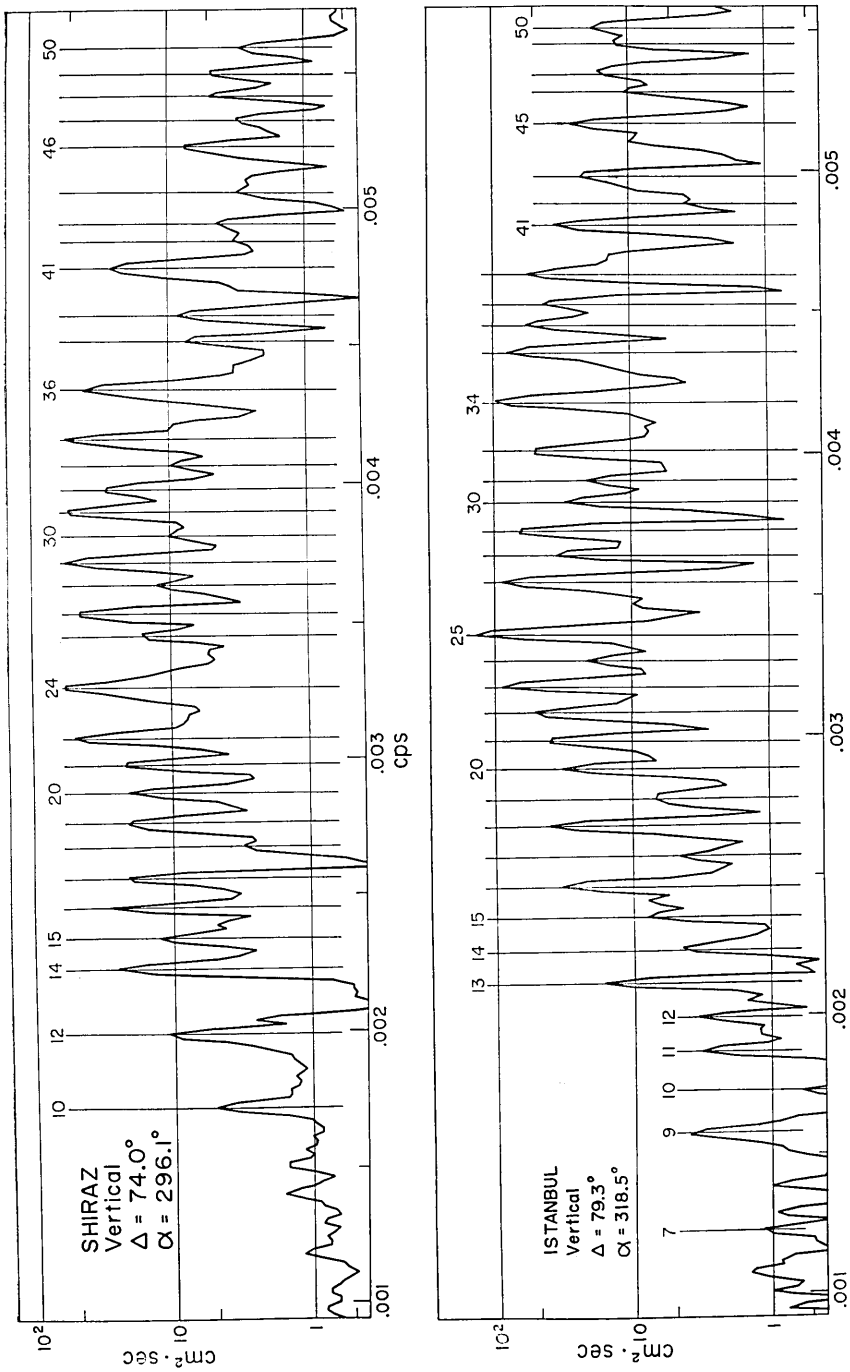

Fig. 4*a*. Power spectral densities of spheroidal oscillations. A kind of normalization was carried out so that the maximum magnification of the instruments may be always 1500. The vertical scale indicates the unit of reading on the original seismogram.

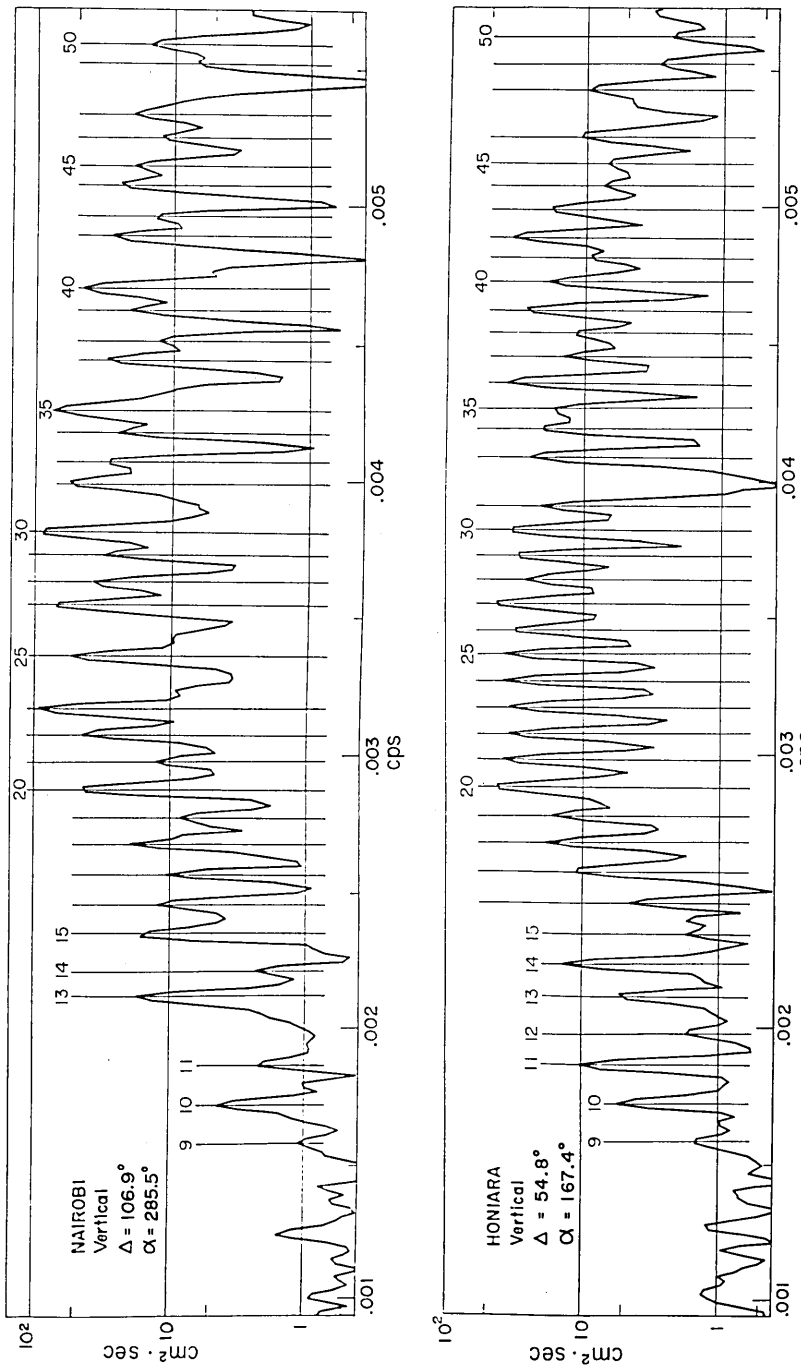

Fig. 4b. Power spectral densities of spheroidal oscillations. A kind of normalization was carried out so that the maximum magnification of the instruments may be always 1500. The vertical scale indicates the unit of reading on the original seismogram.

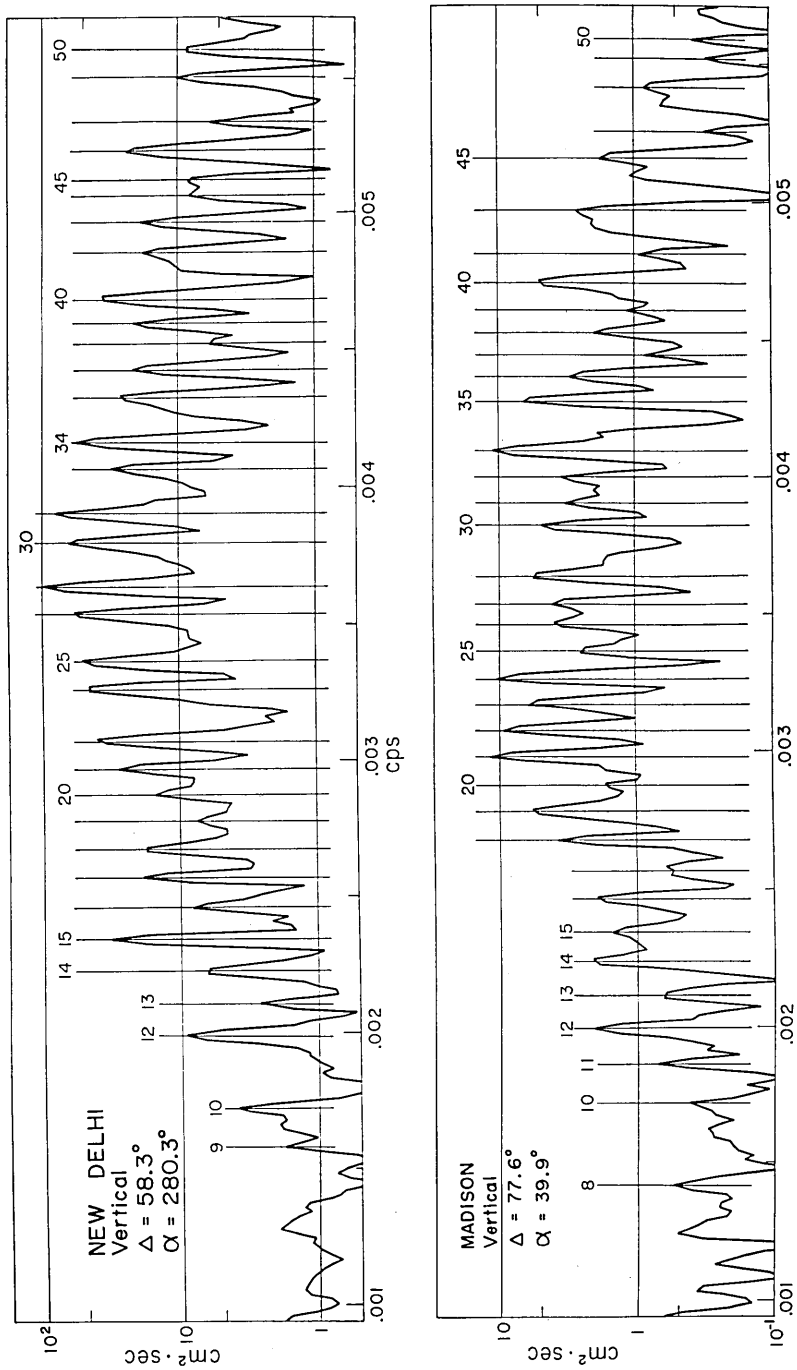

Fig. 4c. Power spectral densities of spheroidal oscillations. A kind of normalization was carried out so that the maximum magnification of the instruments may be always 1500. The vertical scale indicates the unit of reading on the original seismogram.

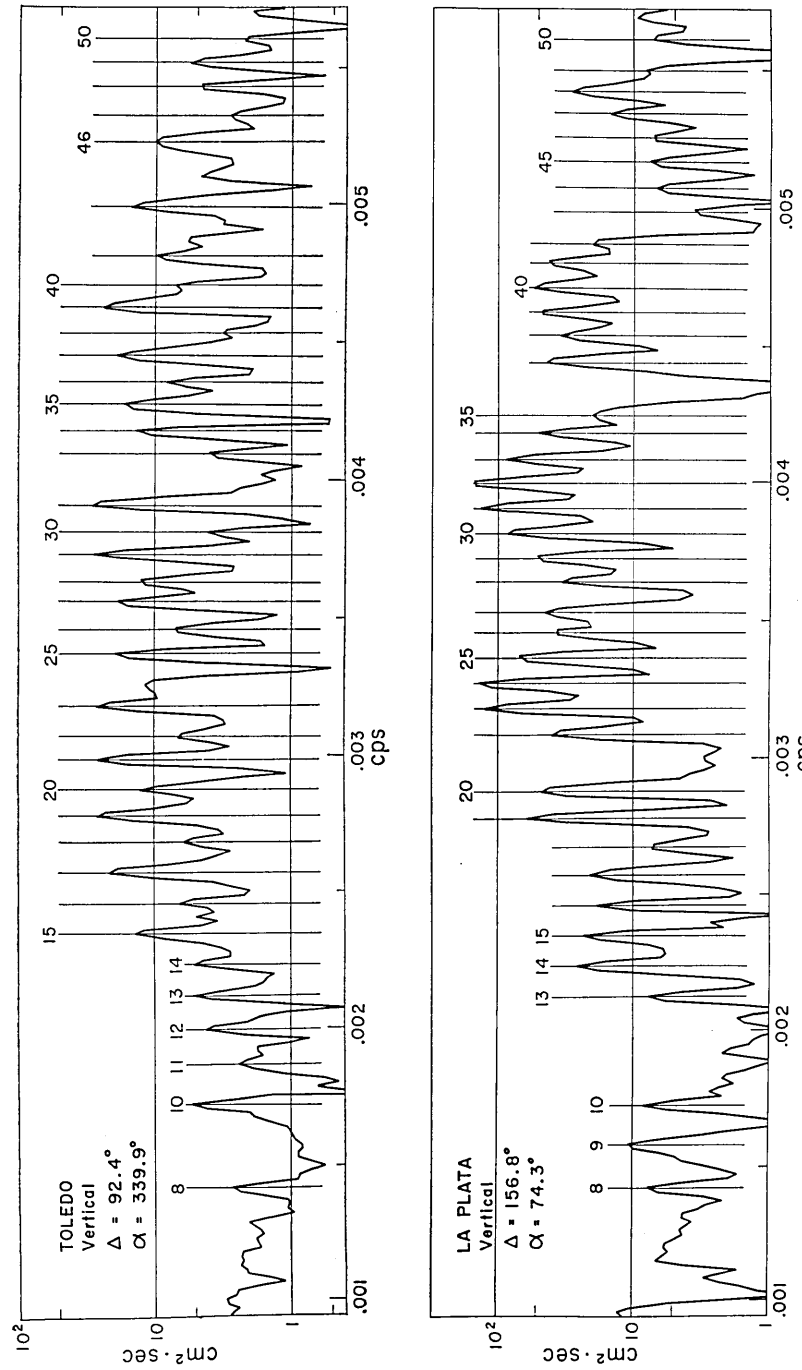

Fig. 4*d*. Power spectral densities of spheroidal oscillations. A kind of normalization was carried out so that the maximum magnification of the instruments may be always 1500. The vertical scale indicates the unit of reading on the original seismogram.

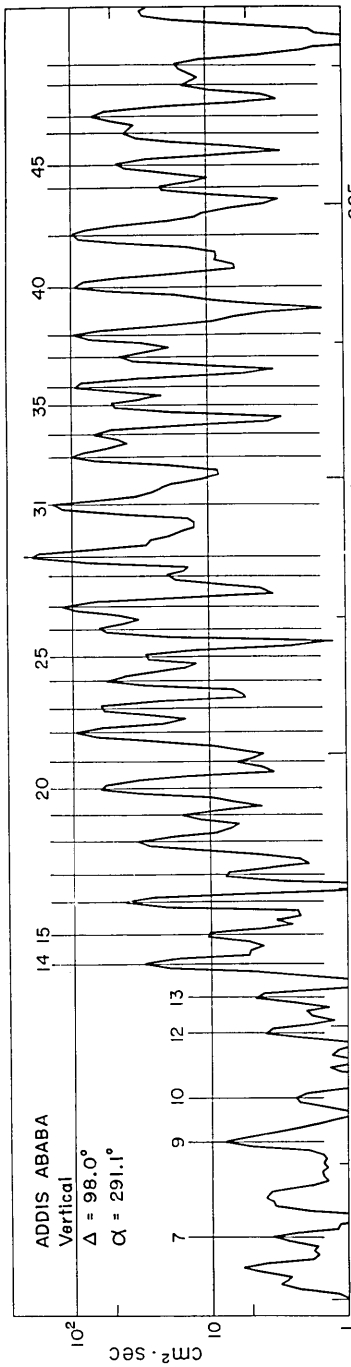

Fig. 4e. Power spectral densities of spheroidal oscillations. A kind of normalization was carried out so that the maximum magnification of the instruments may be always 1500. The vertical scale indicates the unit of reading on the original seismogram.

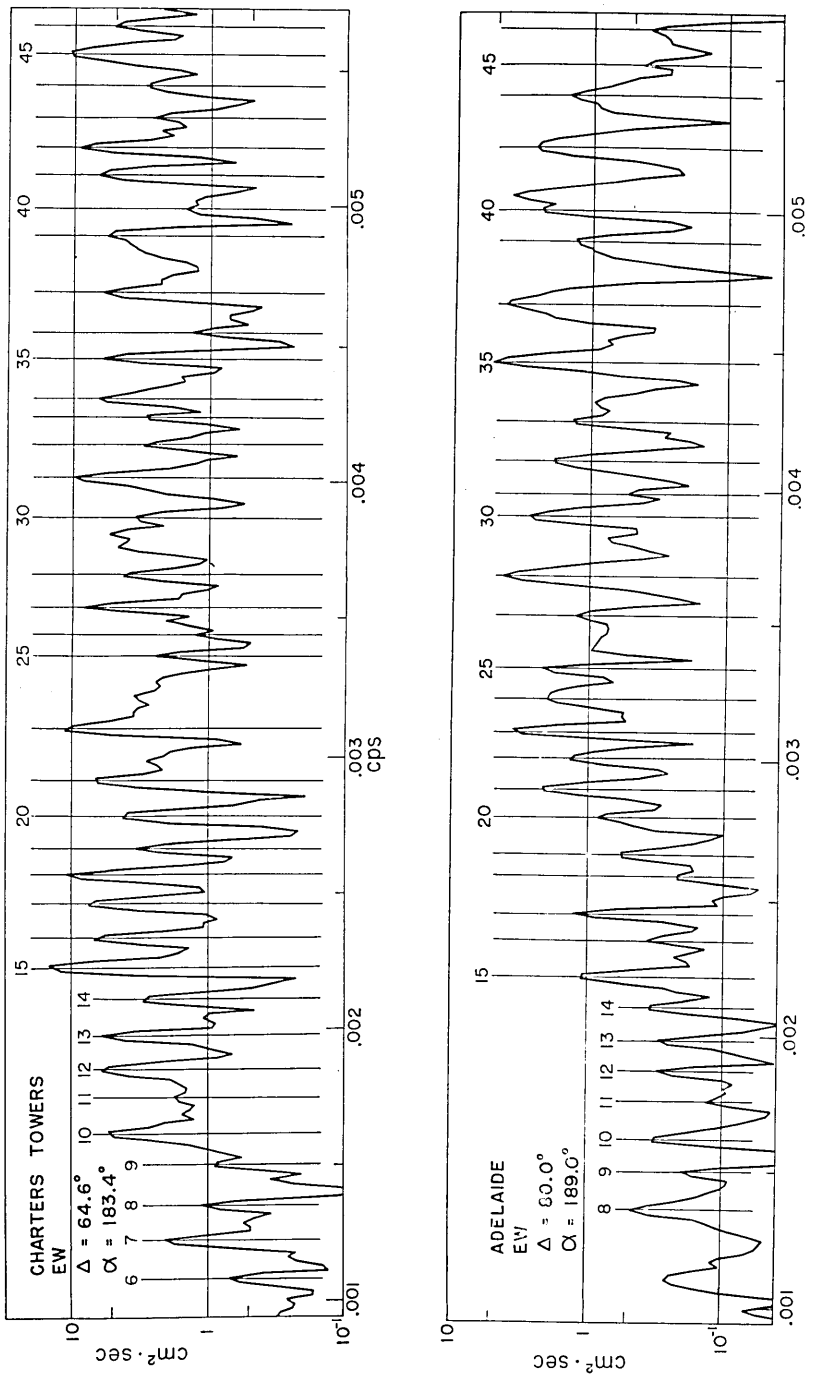

Fig. 4*f*. Power spectral densities of torsional oscillations.

the area surrounded by spectral peaks gives the square of mean amplitudes over the analyzed interval if the effect of the numerical filter is removed.

3. Observed period

Table 2 gives the observed eigen periods of fundamental spheroidal and torsional oscillations obtained from the peaks of power spectra at eleven stations. In the following sections notations S and T stand for the spheroidal and torsional modes, and the suffixes n and m are the parameters of the associated Legendre functions.

The fundamental spheroidal modes from S_7 to S_{50} and fundamental torsional modes from T_7 to T_{46} were detected. The modes lower than S_7 and T_7 were not obtained clearly, probably because of the poor response of pendulum seismographs to such long periods. Owing to the finite length of records, the accuracy in the period determination from the peaks of power spectrum is around $\pm 0.9\%$ for longer periods and $\pm 0.4\%$ for shorter periods.

The theoretical eigen periods for several earth models and observed periods of both S and T modes have been summarized by *Alsop* [1963], *Press* [1964], and *Anderson* [1967]. The observed periods for S_7-S_{50} are almost within 2 sec difference from the theoretical periods of Gutenberg-Bullen A model (hereafter abbreviated to GB-A model). However, the existence of systematic deviations is clear. The observed periods for $S_{11}-S_{14}$ are slightly shorter (about 0.8 sec) compared with theoretical periods of GB-A model. On the contrary, for $S_{18}-S_{50}$ the observed periods are uniformly longer than the theoretical ones by about 1.3 sec. The maximum discrepancy is 2.0 sec at $n=33$. Such a result was reported by *Nagamune et al.* [1964] and can be seen in the works by *Alsop* [1964b] and *Nowroozi* [1965], too. In Fig. 5, we compared other earth models with our observation. It is clear that the model HB1 constructed by *Bullen* and *Haddon* [1967] on the basis of the free oscil-

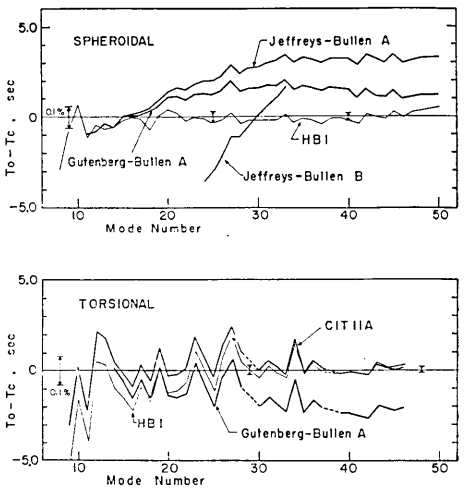

Fig. 5. Deviation of spheroidal and torsional free periods for various earth models from the experimental average values. The periods T_o and T_c designate the experimental and calculated periods respectively. Vertical bars indicate the range of 0.1%.

Table 2. Experimental eigen periods of fundamental spheroidal and torsional oscillations.

OBSERVED PERIODS , IN SEC.

	SPHEROIDAL OSCILLATIONS										TORSIONAL OSCILLATIONS			
N	SHI	IST	NAI	HNR	NDI	MDS	TOL	LPA	AAE	MEAN	N	CTA	ADE	MEAN
7		813.4							814.3	813.9	7	815.4		815.4
8						705.4	705.0	704.5		705.0	8	738.7	736.2	737.5
9		633.1	633.9	632.8	632.9			633.3	633.3	633.2	9	668.0	665.7	666.9
10	580.3	578.9	581.1	580.0	580.2	581.3	581.0	580.6	577.9	580.1	10	618.6	616.5	617.6
11		535.5	536.4	535.4		536.5	536.3			536.0	11	573.4	568.9	571.2
12	501.4	502.0		503.2	501.3	502.2	502.0		503.6	502.2	12	539.0	537.1	538.1
13		472.5	471.8	472.8	474.7	473.8	471.8	471.4	473.2	472.8	13	506.4	504.6	505.5
14	447.7	447.8	448.2	447.5	449.2	446.8	448.2	447.9	447.9	447.9	14	475.7	475.8	475.8
15	426.4	425.6	426.9	426.2	426.2	427.0	426.9	426.5	426.5	426.5	15	450.1	450.2	450.2
16	407.0	406.7	407.5	406.8	406.9	406.3	407.5	407.1	407.1	407.0	16	428.6	425.7	427.2
17	389.3	389.5	389.8	389.0	389.2	389.9	389.7	389.4	390.7	389.6	17	407.7	409.0	408.4
18	373.1	373.6	373.5	372.9	374.1	373.7	373.5	374.3	373.2	373.5	18	390.0	388.7	389.4
19	360.2	360.0	360.7	360.0	360.1	359.7	360.6	360.3	360.3	360.2	19	374.9	374.7	374.8
20	348.2	347.4	347.7	347.1	348.1	347.8	348.6	347.4	348.3	347.8	20	358.8	357.6	358.2
21	336.1	335.6	335.6	335.0	336.9	335.7	335.6		337.1	336.0	21	344.0	344.8	344.4
22	324.7	324.5	325.2	324.6	324.6	325.3	326.0	324.9	324.9	325.0	22		332.0	332.0
23		315.0	315.4	314.8		315.5	315.3	315.1	315.9	315.3	23	322.8	320.9	321.9
24	306.5	306.0		305.6	306.4	306.2		305.9	305.9	306.1	24		309.8	309.8
25		297.5	297.4	296.9	297.0	297.5	297.4	297.2	297.9	297.4	25	297.6	299.4	298.5
26	289.5			289.3		289.3	289.2	289.6	290.3	289.5	26	290.7		290.7
27	283.0	281.8	282.0	281.8	282.9	282.8	282.0	283.7	282.4	282.5	27	282.8	282.5	282.7
28	274.9	274.0	275.2	274.8	274.8	274.7	275.2	275.0	274.7	274.8	28	273.0	272.7	272.9
29	269.0	268.3	268.2	268.3			268.2	267.9	268.5	268.3	29			
30	262.2	261.2	262.0	261.6	262.2	261.6	262.5	262.3		262.0	30		256.5	256.5
31	256.3	256.0		255.7	255.7	256.2	256.1	255.9	255.9	256.0	31	249.2	250.8	250.0
32	251.2	249.6	250.5			250.1		250.3		250.3	32	242.4	243.5	243.0
33	245.8		245.6	244.7	245.7	244.3	244.6	244.9	244.9	245.1	33	236.5	236.1	236.3
34	240.1	238.9	239.5	238.6	240.1		239.5	239.3	240.2	239.5	34	232.1		232.1
35			235.0	234.6		234.2	234.1	235.7	234.4	234.7	35	225.0	224.3	224.7
36	230.4	229.5		229.5	230.4	229.1	229.8		230.1	229.8	36	219.9		219.9
37		224.7	224.9	224.5	225.4	225.0	224.9	225.5	225.1	225.0	37	214.3	214.3	214.3
38	220.1	220.8	221.7	220.2	220.6	221.0	220.9	220.8	220.8	220.8	38			
39	216.9	215.6	216.4	216.4	216.8	217.2	216.0	216.6		216.5	39	204.5	204.2	204.4
40			212.7	211.6	212.4	212.4	212.7	212.5	212.5	212.4	40	200.3	199.6	200.0
41	208.9	208.0		207.8		207.9	207.8	208.3		208.1	41	195.6		195.6
42	204.8	204.7	204.4	204.7	205.4			204.9	204.6	204.8	42	192.0	190.8	191.4
43	201.9	200.8	201.5	200.5	200.8	201.2	200.2	200.3		200.9	43	188.0		188.0
44	197.7		197.0	197.0	197.0			197.2	197.5	197.2	44	183.9	184.0	184.0
45		193.6	194.3	193.9	195.2	193.8		193.5	194.1	194.1	45	180.2	180.3	180.3
46	191.4	189.6	190.2	190.1	191.0	190.2	191.3	190.3	190.0	190.5	46	176.9	176.8	176.9
47	187.6	187.3	187.3		197.0		187.9	187.2	187.7	187.4				
48	184.9			184.2		184.6	184.3	184.4	183.9	184.4				
49	181.9	181.5	180.8	181.1	181.6	180.9	181.4	181.7	181.5	181.4				
50	179.1	178.0	178.8	177.7	178.3	178.8	178.8	178.1		178.5				

lation data, shows a good agreement with our results, 0.1% for $S_{10}-S_{50}$. Theoretical periods and corresponding phase velocities of HB1 model for the spheroidal as well as torsional modes, are presented in another paper by *Haddon* and *Bullen* [1969].

The average observed periods of torsional oscillations for $T_{15}-T_{46}$ are uniformly shorter compared with the theoretical periods of GB-A, and the discrepancy increases toward shorter periods (see Fig. 5). The CIT 11A model, which provides a good fit with the observation, has been determined by *Anderson* and *Toksöz* [1963] and *Kovach* [1965] mainly from the long period oceanic Love wave data, and has a shallower low-velocity zone in the upper mantle. As far as the free oscillation is concerned, the model HB1 satisfies the observation best for the period range analyzed here.

4. Observed phase velocity

Since the equivalent phase velocity is uniquely determined from the period, essentially speaking, the discussion about the dispersion curve hardly exceeds what was discussed in the previous section about the period. As a propagating wave, the equivalent phase velocity C of a mode with the order number n is derived from the free oscillation period T by

$$C=(2\pi a)/[(n+1/2)T]\ , \tag{4.1}$$

where a is the earth's radius, assumed to be 6371 km. This formula is based on the asymptotic expansion of the Legendre function with large n, and valid outside of the vicinity of the epicenter and the antipode. Table 3 gives the observed phase velocities of both types of fundamental modes at each station.

The phase velocity dispersion curves are shown in Figs. 6, 7 and 8 using the average periods as obtained from the observed data. The vertical bars in these figures show the uncertainty due to the finiteness of the records. The accuracy of the observed phase velocity is, as seen in the figures, about 0.9% and 0.4% for the longer and shorter periods respectively.

For spheroidal modes, or Rayleigh waves as propagating waves, the observed phase velocities appear to be slightly, but consistently lower for periods shorter than 350 sec, and slightly higher in the period range from 440 to 540 sec than those for GB-A model (Fig. 6). The discrepancy is of the order of 0.03 km/sec for $T=180-350$ sec, and 0.01 km/sec for $T=440-540$ sec. The observed phase velocities are in good agreement with the theoretical values of GB-A model in the period range from 370 to 430 sec. As mentioned before, however, HB1 model best explains

Table 3. Experimental phase velocities of fundamental spheroidal and torsional oscillations calculated from free oscillation periods. The mean values correspond to the mean free periods.

OBSERVED PHASE VELOCITIES , IN KM/SEC.

SPHEROIDAL OSCILLATIONS

N	SHI	IST	NAI	HNR	NDI	MDS	TOL	LPA	AAE	MEAN
7		6.562							6.555	6.558
8						6.676	6.680	6.685		6.680
9		6.656	6.647	6.659	6.658			6.654	6.654	6.655
10	6.570	6.586	6.561	6.573	6.571	6.558	6.562	6.566	6.597	6.572
11		6.500	6.489	6.501		6.488	6.491			6.494
12	6.387	6.379		6.364	6.388	6.377	6.379		6.359	6.377
13		6.276	6.285	6.272	6.246	6.258	6.285	6.290	6.266	6.272
14	6.166	6.165	6.160	6.169	6.146	6.179	6.160	6.164	6.164	6.164
15	6.057	6.063	6.050	6.060	6.060	6.048	6.050	6.055	6.055	6.055
16	5.961	5.965	5.954	5.964	5.962	5.971	5.954	5.959	5.959	5.961
17	5.876	5.873	5.868	5.880	5.877	5.867	5.870	5.874	5.855	5.871
18	5.800	5.792	5.793	5.803	5.784	5.790	5.793	5.781	5.798	5.793
19	5.699	5.702	5.691	5.702	5.701	5.707	5.693	5.698	5.698	5.699
20	5.608	5.621	5.616	5.626	5.610	5.614	5.602	5.621	5.606	5.614
21	5.540	5.548	5.548	5.558	5.526	5.546	5.548		5.523	5.541
22	5.479	5.483	5.471	5.481	5.481	5.469	5.457	5.476	5.476	5.474
23		5.408	5.401	5.411		5.399	5.403	5.406	5.392	5.403
24	5.331	5.339		5.346	5.333	5.336		5.341	5.341	5.338
25		5.277	5.278	5.287	5.286	5.277	5.278	5.282	5.270	5.278
26	5.218			5.221		5.221	5.223	5.216	5.203	5.218
27	5.144	5.166	5.162	5.166	5.145	5.147	5.162	5.131	5.155	5.153
28	5.109	5.126	5.104	5.111	5.111	5.113	5.104	5.108	5.113	5.111
29	5.044	5.058	5.059	5.058			5.059	5.065	5.054	5.058
30	5.006	5.025	5.009	5.017	5.006	5.017	5.000	5.004		5.009
31	4.958	4.964		4.970	4.970	4.960	4.962	4.966	4.966	4.964
32	4.903	4.935	4.917			4.925		4.921		4.921
33	4.861		4.865	4.883	4.863	4.891	4.885	4.879	4.879	4.875
34	4.833	4.857	4.845	4.863	4.833		4.845	4.849	4.831	4.845
35			4.798	4.807		4.815	4.817	4.784	4.811	4.804
36	4.760	4.779		4.779	4.760	4.787	4.772		4.766	4.772
37		4.751	4.746	4.755	4.736	4.744	4.746	4.734	4.742	4.744
38	4.724	4.709	4.690	4.722	4.713	4.705	4.707	4.709	4.709	4.709
39	4.672	4.700	4.683	4.683	4.674	4.666	4.692	4.679		4.681
40			4.647	4.671	4.653	4.653	4.647	4.651	4.651	4.653
41	4.617	4.637		4.642		4.640	4.642	4.631		4.635
42	4.599	4.601	4.608	4.601	4.586			4.597	4.604	4.599
43	4.558	4.583	4.567	4.590	4.583	4.574	4.597	4.594		4.581
44	4.550		4.566	4.566	4.566			4.562	4.555	4.562
45		4.544	4.528	4.537	4.507	4.540		4.547	4.533	4.533
46	4.498	4.540	4.526	4.528	4.507	4.526	4.500	4.524	4.531	4.519
47	4.492	4.499	4.499		4.507		4.485	4.502	4.490	4.497
48	4.464			4.481		4.471	4.478	4.476	4.488	4.476
49	4.446	4.456	4.473	4.465	4.453	4.470	4.458	4.451	4.456	4.458
50	4.426	4.453	4.433	4.461	4.446	4.433	4.433	4.451		4.441

TORSIONAL OSCILLATIONS

N	CTA	ADE	MEAN
7	6.546		6.546
8	6.375	6.397	6.386
9	6.308	6.330	6.318
10	6.163	6.184	6.173
11	6.071	6.119	6.094
12	5.941	5.962	5.951
13	5.855	5.876	5.866
14	5.803	5.802	5.802
15	5.738	5.737	5.737
16	5.660	5.699	5.679
17	5.611	5.593	5.601
18	5.548	5.567	5.557
19	5.476	5.479	5.477
20	5.442	5.461	5.451
21	5.412	5.400	5.406
22		5.359	5.359
23	5.277	5.308	5.292
24		5.274	5.274
25	5.275	5.243	5.259
26	5.196		5.196
27	5.147	5.153	5.149
28	5.145	5.151	5.147
29			
30		5.117	5.117
31	5.100	5.067	5.083
32	5.081	5.058	5.069
33	5.053	5.061	5.057
34	4.999		4.999
35	5.012	5.027	5.018
36	4.987		4.987
37	4.981	4.981	4.981
38			
39	4.956	4.963	4.958
40	4.935	4.952	4.942
41	4.931		4.931
42	4.906	4.937	4.921
43	4.895		4.895
44	4.892	4.889	4.889
45	4.882	4.880	4.880
46	4.866	4.869	4.866

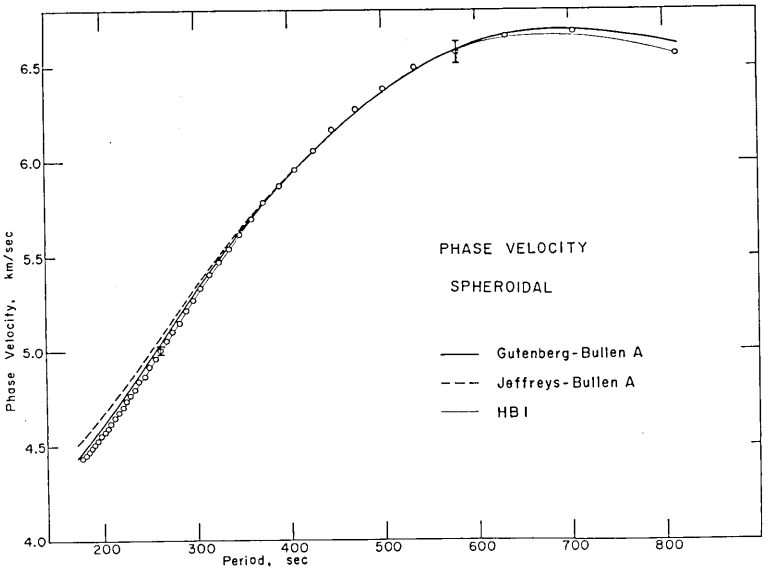

Fig. 6. Experimental phase velocities of spheroidal modes compared with those of several earth models. Vertical bars indicate the uncertainty in the period determination due to the finiteness of the record.

the data for periods shorter than 430 sec; only a slight discrepancy exists for periods longer than 440 sec as well as for GB-A model.

The phase velocities for the two paths through SHI and HNR are

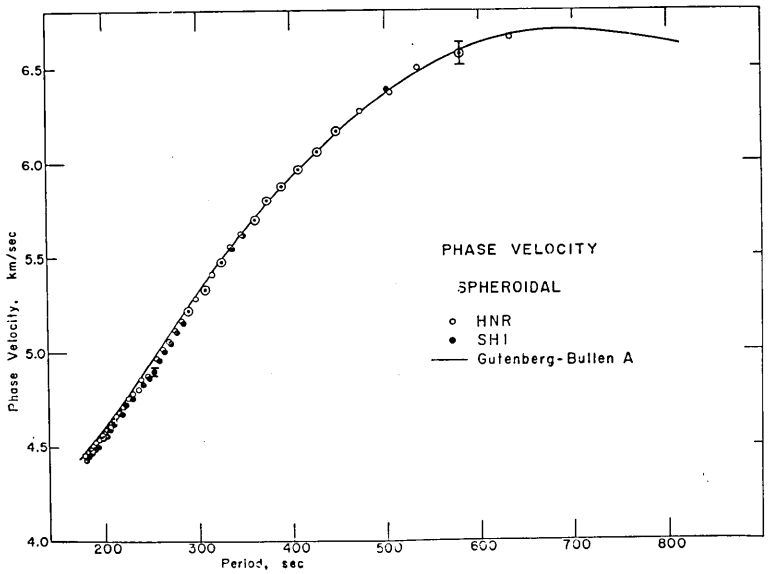

Fig. 7. Experimental phase velocities at SHI and HNR from the free oscillation periods of spheroidal modes. The great circle paths to SHI and HNR contain 60% and 80% oceanic parts respectively.

shown in Fig. 7. The great circle paths through SHI and HNR contain 60% and 80% oceanic parts respectively. For periods longer than 360 sec, two observations give fairly close values, but the divergence starts around this period and becomes significant toward short periods. This observed difference among the paths is of the order of 0.03 km/sec or 0.7% at $T=200$ sec, and the phase velocity at HNR is appreciably higher than that at SHI. Generally speaking, in the period range discussed here, the phase velocity of propagating waves through oceanic regions is higher than that through continents which have no significant shield regions. Such difference in phase velocity is 0.5% to 1% for $T=600-200$ sec [*Toksöz* and *Anderson*, 1966; *Derr*, 1967]. The structure of the upper mantle varies markedly among various regions such as ocean, shield, and tectonic areas [*e.g. Båth*, 1965; *Kanamori*, 1970]. It seems almost certain that such a large regionality in the upper mantle affects at least high order free oscillations of the earth.

This can be interpreted as follows: For a spherically symmetric earth a peak of power spectrum corresponding to one mode of oscillation contains unresolved components which are degenerated with respect to azimuthal order number m. The lateral heterogeneity of any kind will remove this degeneracy and produce a multiplet in the spectrum [*Backus* and *Gilbert*, 1961]. The asymmetrical excitation with respect to m complicates the relative amplitude of the individual lines in the multiplet, because in general the excitation of free oscillations depends on a geometry of the source. However, in case the spacing between adjacent split lines is smaller than the line broadening due to the finite length of the record, the dissipation, and the noise [*Gilbert* and *Backus*, 1965; *Smith*, 1966], the multiplet will produce in the spectrum a single broad line. For high order modes one observes only the envelope of the multiplet by broadening the individual lines, so that the apparent center of this envelope which depends on the relative location of the source and the receiver, will not correspond to the frequency for the spherically symmetric earth. The divergence between the observations for the path through SHI, and for the path through HNR, becomes significant for periods shorter than 350 sec. This period can be interpreted as a depth to which the significant lateral variations of any kind will exist in the upper mantle not deeper than several hundred kilometers.

For torsional modes, or Love waves as propagating waves, the observed phase velocities are consistently higher toward shorter periods from 450 sec than those of GB-A model and rather close to those of CIT 11A model, although the observed values scatter appreciably (Fig. 8). This scatter may be due to the contamination of spheroidal modes to the transverse component. Both CTA and ADE lie on a great circle path with 70% oceanic part.

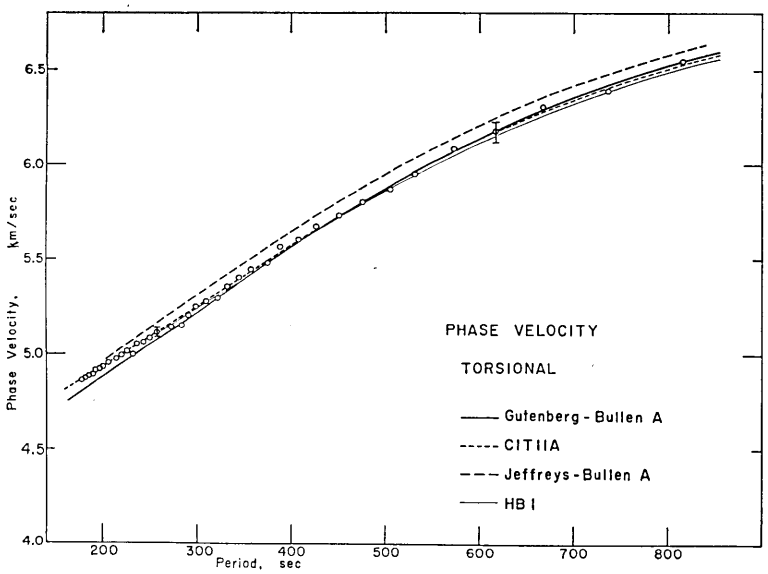

Fig. 8. Experimental phase velocities of torsional modes compared with those of several earth models.

HB1 model can also explain the observations of torsional modes for periods shorter than 440 sec. However, for both types of modes, especially in torsional modes, a slight discrepancy exists for periods longer than 440 sec, the GB-A model being superior to HB1 in this period range.

5. Attenuation of free oscillations

The amplitude of a mode of free oscillation at the time t is expressed by

$$A(t)=A(t_0)\exp\left[-\pi(t-t_0)/QT\right], \tag{5.1}$$

from which the Q factor can be computed by measuring the rate of the decay of spectral amplitudes with time. The rate of decay is ordinarily estimated by the comparison of two corresponding peaks in two time ranges [*Ness et al.*, 1961].

The decay of the spheroidal oscillations has been studied by separate spectrum analysis of two intervals of 10 hours. The spectrum analysis as stated before was employed for six stations SHI, IST, NAI, HNR, LPA and AAE. The Q factor of each mode was determined from the ratio of the mean amplitude in the individual 10-hour intervals. A summary of average values of Q at these stations is given in Table 4 and is also plotted against the period in Fig. 9 for each mode. Despite the

Table 4. A summary of average Q factors of spheroidal oscillations and the time interval of data used in the analysis.

Station	To* (min)	Q ($S_{13}\sim S_{17}$)	Q ($S_{18}\sim S_{42}$)
SHI	593.0	275	198
IST	580.1	233	199
NAI	593.8	284	161
HNR	592.7	238	224
LPA	593.3	243	239
AAE	593.3	262	163
Average		251±30	200±49

* Time interval of each segment.

scattering of the data, the value of Q tends to increase with the period, namely

$$Q=251\pm30 \text{ for } S_{13}-S_{17} \text{ (or } T=380-480 \text{ sec)},$$

$$Q=200\pm49 \text{ for } S_{18}-S_{42} \text{ (or } T=200-380 \text{ sec)}.$$

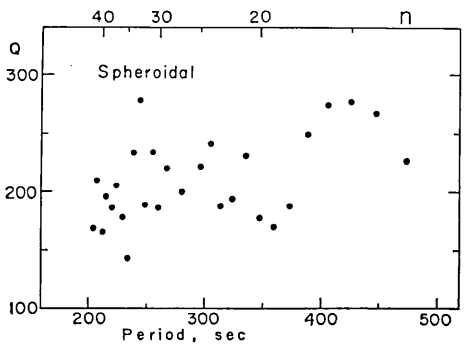

Fig. 9. Experimental Q factors for spheroidal oscillations.

Nowroozi [1968] obtained the value 251±42 for the spheroidal mode of the Alaskan shock over the period range from 300 to 600 sec, and our result for the range 380 to 480 sec is very close.

The results in Table 4 are almost in accord with other observed data by many investigators [*Connes et al.*, 1962; *Nagamune et al.*, 1964; and see the review by *Sato*, 1967, also].

6. Amplitude variations

The vertical displacement of spheroidal modes is proportional to the associated Legendre function $P_n^m(\cos\theta)$, while azimuthal component of torsional modes to the derivative $dP_n^m(\cos\theta)/d\theta$. The epicenter is assumed to be at the pole of the sphere so that the angle θ, colatitude, gives the epicentral distance. The integers n and m determine the displacement field of a free oscillation on the spherical surface. The number of nodal lines of displacement in θ direction is $n-m$, and that in the azimuthal direction is $2m$. The azimuthal order number m generally does not affect the period, and the spectral lines degenerate with

respect to m for a non-rotating, spherical earth. These unresolved spectral lines for extremely low order modes split due to the rotation of the earth [*MacDonald* and *Ness*, 1961; *Backus* and *Gilbert*, 1961; *Pekeris et al.*, 1961; *Benioff et al.*, 1961]. However, as was also mentioned before, for high order modes the observed single spectral line generally contains unresolved components for azimuthal order number m, because of the finite length of records, the attenuation, and the noise.

A simple method to determine the m value in the unresolved multiplets is the comparison between the vanishing points in the tesseral harmonics and the missing peaks in the observed spectra [*Satô* and *Usami*, 1963]. For this purpose, we, following *Satô* and *Usami* [1963], calculated the zero point curves of $P_n^m(\cos\theta)$ function and its somewhat modified forms for $n=1-50$, $m=0$, 1 and 2 (Figs. 10*a*, *b*, *c*, *d*). The cross points of lines associated with n and θ show the k-th vanishing points of these functions. If the order number n, m and the colatitude θ are fixed, we can determine whether the specified amplitude vanishes or not.

The displacement field of an oscillation can be determined by the equivalent force system of dislocation, and it is assumed here that the dependence on azimuthal order number is limited to 0, 1 and 2. For example, the vanishing modes expected at NAI between $n=9$ and 40 are $n=16$, 21, 26, 31, 36 for $m=0$ or 2, and 10, 15, 27, 32, 37 for $m=1$.

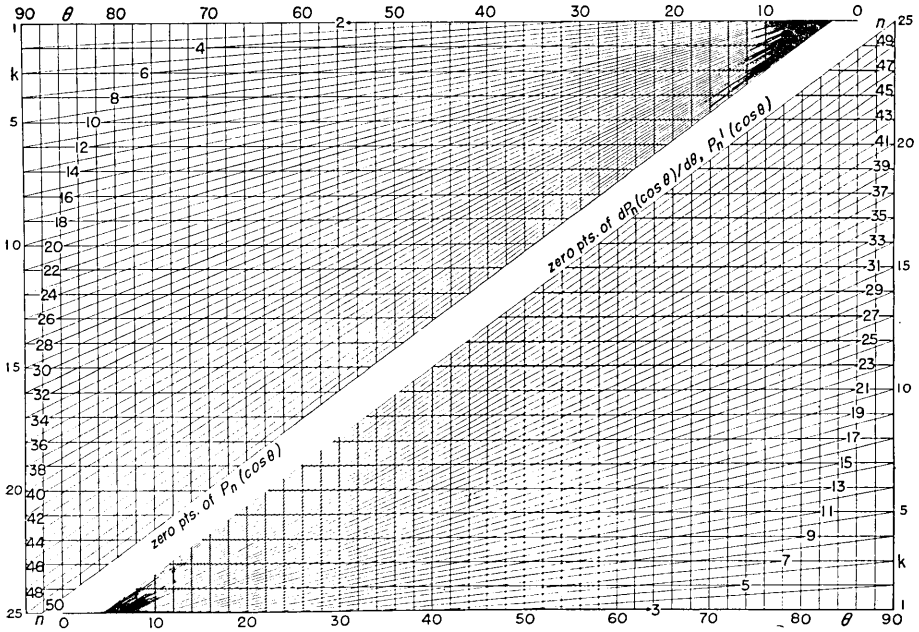

Fig. 10*a*. Zero points of $P_n^m(\cos\theta)$ and its modified functions. The cross point of slant and vertical lines gives k-th zero point of the respective function.

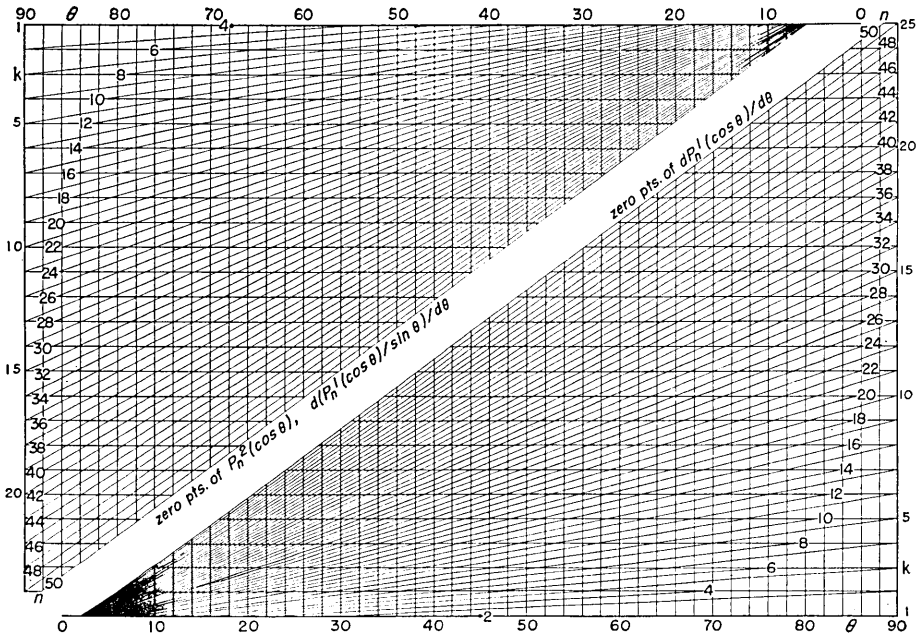

Fig. 10*b*. Zero points of $P_n^m(\cos\theta)$ and its modified functions. The cross point of slant and vertical lines gives k-th zero point of the respective function.

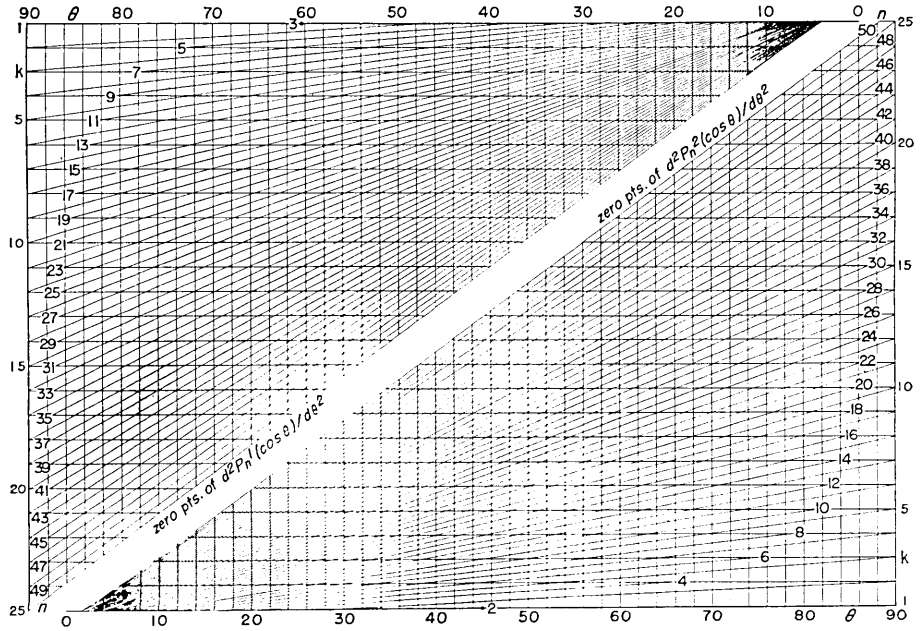

Fig. 10*c*. Zero points of $P_n^m(\cos\theta)$ and its modified functions. The cross point of slant and vertical lines gives k-th zero point of the respective function.

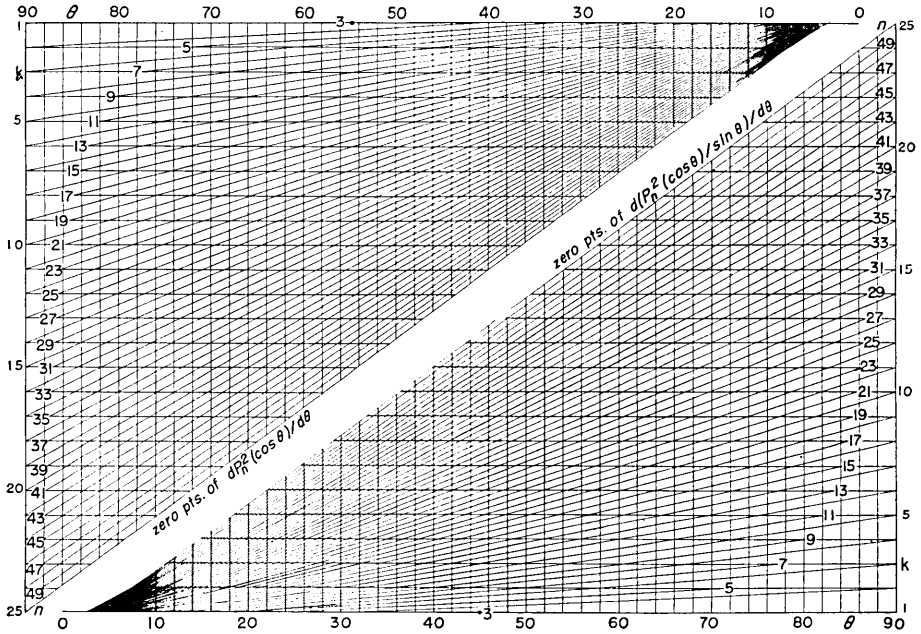

Fig. 10*d*. Zero points of $P_n^m(\cos\theta)$ and its modified functions. The cross point of slant and vertical lines gives k-th zero point of the respective function.

On the other hand, the observed missing peaks are $n=12$, 24, 26, 31 and 36. Accordingly the orders 26, 31, 36 coincide well for $m=0$ or 2, but others 12, 24 coincide neither with $m=0$, 2 nor 1.

Table 5 gives the result of comparison between the theoretical vanishing points and observed missing peaks over the range of $n=9-40$ in all the spectra of eleven stations. According to this table, the existence of the modes $m=0$ and 2 is almost certain, while that of the mode $m=1$ is questionable, although there are some missing peaks that cannot be ascribed to any of the orders $m=0$, 1 or 2. These undefined missing peaks might have been caused either by the finiteness of the fault, or

Table 5. Comparison between the zero points of P_n^m functions and the missing peaks of observed spectra for $n=9-40$.

	Spheroidal	Torsional
N_m*	29	5
$m=0,2$	16	4
$m=1$	1	1
Undefined	12	0

* N_m is the total number of observed missing peaks for $n=9-40$.

the ellipticity and heterogeneity of the earth. When n is large we can hardly separate the mode $m=0$ from $m=2$ because of the closeness of vanishing points in the domain not far from the equator. The source mechanism of the earthquake has been determined by the comparison between the observed and the theoretical radiation patterns for long-period surface waves by *Kanamori* [1969]. He concluded that the source of the earthquake is predominantly pure dip-slip with a dip angle at 22°. In this case, the excitation of free oscillation is almost limited to $m=0$ and 2 for the spheroidal and to $m=2$ for the torsional modes.

7. Distribution of spectral amplitude on the earth's surface

Since we obtained the spectral amplitude at a number of stations, we can expand them into a series of spherical surface harmonics of the form

$$|F_n^i(\theta, \phi)| = A_0 + A_n P_n(\cos\theta) + P_n^2(\cos\theta)\cdot(B_n^2 \cos 2\phi + C_n^2 \sin 2\phi) \ , \qquad (7.1)$$

where $|F_n^i|$ is the observed amplitude of spheroidal oscillations for the n-th mode at i-th station, ϕ the azimuth as seen from the source to the station. Amplitudes were corrected for the attenuation assuming the value

$$Q = \begin{cases} 300 & \text{for} \quad S_9 - S_{15} \\ 200 & \text{for} \quad S_{16} - S_{50} \ , \end{cases}$$

and were reduced to the time of earthquake occurrence;

$$|F_n^i| = \frac{\gamma T_0}{\exp(-\gamma t_0)\cdot[1-\exp(-\gamma T_0)]} \cdot \bar{U}_m \ , \qquad (7.2)$$

where $\bar{U}_m$ is the mean displacement amplitude of the ground at the point of observation over the time interval T_0, $\gamma = \pi/QT$, T the period, and t_0 is the starting time of the analyzed record. For this calculation six stations SHI, IST, NAI, HNR, NDI and TOL were used. The equation (7.1) is a linear algebraic equation with unknowns A_0, A_n, B_n^2 and C_n^2, and there are six equations of this type for each mode n. Hence, the coefficients can be determined by applying the method of least squares.

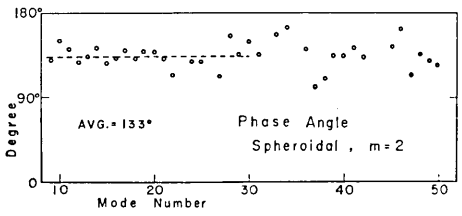

Fig. 11. Phase angle ψ for the expansion of spectral amplitudes into the spherical surface harmonics. The angle N133°E fits the dip direction of the earthquake fault.

Figure 11 shows the phase angle ψ defined by the expression

$$P_n^2(\cos\theta)\cdot(B_n^2\cos 2\phi + C_n^2\sin 2\phi) = D_n^2\cdot P_n^2\cos[2(\phi-\psi)]\ . \tag{7.3}$$

The average value of ψ calculated in this way gives N133°E±13° in the range $n=9-30$, and this angle corresponds to the direction for the maximum amplitudes of P_n^2 term. The source mechanism of this Kurile Islands earthquake will be assumed as a double couple with a pure dip-slip motion on a fault dipping at 45° [*Abe*, 1969]. In this mechanism, the components of $m=0$ and 2 are excited for the spheroidal oscillations. The theoretical radiation pattern for the component of $m=2$ has two spatial orientations of maximum amplitude, in which one is the strike of the fault and another is the dip direction of the fault. *Stauder* and *Bollinger* [1966] and *Kanamori* [1969] obtained the dip direction of the fault of N133°E for the earthquake, and this direction of N133°E is in good agreement with our observation. Figure 12 shows the ratio of the coefficients $D_n^2/|A_n^0|$, where D_n^2 is the maximum amplitude for P_n^2 term, and A_n^0 for P_n^0 term. This corresponds to the spectral ratio of the excitation for $m=0$ and $m=2$. Although the observed data scatter slightly, the major feature is consistent with the theoretical value expected from the amplitude excitation for the 45° dip-slip type earthquake. The basic formula has been given by *Saito* [1967]. A further study on the amplitude of the free oscillation and its excitation is carried out with Saito's method by *Abe* [1969].

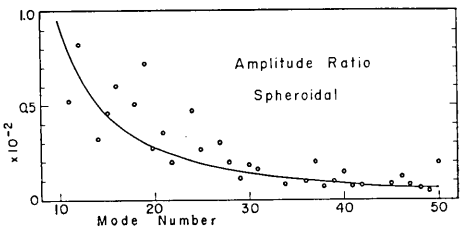

Fig. 12. Amplitude ratio as a function of order number n, $|D_n^2/A_n|$. Solid curve shows the theoretical result derived from the assumption that the source mechanism is a double couple with a pure dip-slip motion on a fault dipping at 45°. A step source time function is also assumed (see e.g. *Abe* [1969]).

8. Phase angle of free oscillations

The free oscillation of the earth is, if the medium is laterally homogeneous, expressed by a formula of the form

$$u = A\cdot R_n(r)\cdot Y_n^m(\theta,\phi)\cdot\exp(ip_n t)\ , \tag{8.1}$$

where u is a displacement component,

R_n is a function of r with a parameter n,

$Y_n^m(\theta,\phi)$ is the spherical surface harmonics or its modified form with parameters n and m,

p_n is an eigen frequency,

and A is a quantity independent of θ and ϕ [*Satô et al.*, 1967, 1968].

If this equation holds, the complex amplitudes at various stations corresponding to an oscillation with the eigen frequency p_n should have phase angles with difference of integral multiples of π.

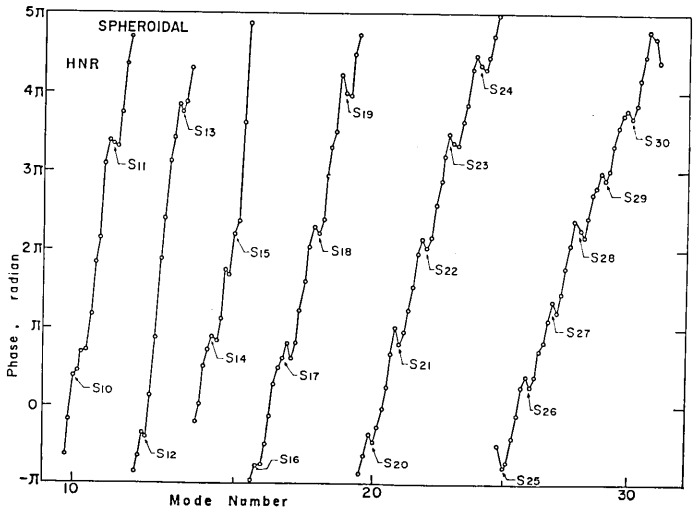

Fig. 13*a*. Phase angle of free oscillations reduced to the time of earthquake occurrence at HNR. The epicentral distance is 54.8°.

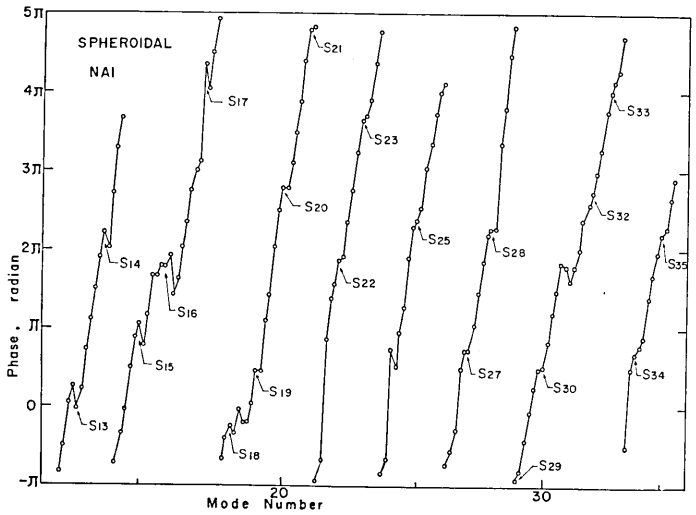

Fig. 13*b*. Phase angle of free oscillations at NAI. The epicentral distance is 106.9°.

Figures 13*a*, *b* show the phase angles reduced to the time of earthquake occurrence. The phase difference at two stations is rather irregular (see Fig. 14). Although we are unable to explain the cause of this

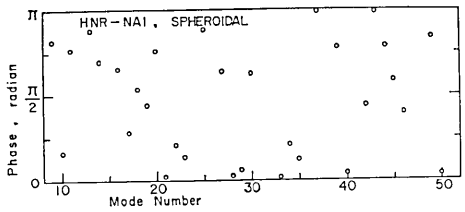

Fig. 14. Phase difference between HNR and NAI.

scatter, it is possible that the source finiteness and the lateral inhomogeneity of any kind may disturb the observed phase.

9. Conclusions

Various analyses have been made on the spectral peaks, amplitudes, and phases of the free oscillations of the earth. The following conclusions can be derived.

For the spectral peaks: (i) The experimental eigen periods and equivalent phase velocities have been determined over the range S_7 to S_{50} or 820 to 170 sec for spheroidal modes, and over the range T_7 to T_{45} or 820 to 170 sec for torsional modes. These sets of data are tabulated individually for eleven stations. (ii) As far as the free oscillation is concerned, the model HB1 satisfies the observation best. (iii) The observational data for the path through different stations, however, appear to be slightly different, and such divergence becomes significant for periods shorter than 350 sec. It is found that they vary in such a way as to reflect the existence of the significant lateral inhomogeneity of any kind in the upper mantle not deeper than several hundred kilometers.

For the amplitudes: (i) The Q factors for spheroidal modes have also been determined from the amplitude decay with time. (ii) The azimuthal order number m has been found to be either 0 or 2 from the zero point of the amplitudes of spectral peaks. For this purpose, we have calculated the zero point curves of $P_n^m(\cos\theta)$ function and its somewhat modified forms for $n=1-50$, $m=0$, 1 and 2. (iii) The spectral amplitudes of the spheroidal modes have been expanded into terms of the spherical harmonics. The direction for the maximum amplitudes of P_n^2 term and the ratio of coefficients for P_n^0 term and P_n^2 term have been determined. The results from (ii), (iii) are consistent with the results expected from the earthquake mechanism and excitation of waves.

For the phases: For a search of any significant pattern of the free oscillation modes of the sphere, the phase difference at two stations has been compared. However, the phase difference thus obtained shows fairly irregular values, and it may be possible that the source finiteness

ellipticity, and lateral inhomogeneity disturb the observed phase. Much is to be expected from the free oscillation amplitudes, which seem to be more stable than phases.

Acknowledgments

We wish to thank Dr. Hiroo Kanamori who kindly provided us with a number of seismograms. We are also very grateful to him for kindly reading the manuscript and giving us various comments. We benefited from discussions with Drs. Tatsuo Usami, Masanori Saito, and Stewart W. Smith in the early stages of this work. Miss Itsue Ochi assisted us in the preparation of the data in digital form and the drawings.

References

ABE, K., Estimation of seismic moment and wave energy from the earth's free oscillation, *Bull. Earthq. Res. Inst.*, **47** (1969), in preparation.

ALSOP, L.E., Free spheroidal vibrations of the earth at very long periods, Part I—Calculation of periods for several earth models, *Bull. Seism. Soc. Am.*, **53** (1963), 483-501.

ALSOP, L.E., Excitation of free oscillations of the earth by the Kurile Islands earthquake of 13 October 1963, *Bull. Seism. Soc. Am.*, **54** (1964a), 1341-1348.

ALSOP, L.E., Spheroidal free periods of the earth observed at eight stations around the world, *Bull. Seism. Soc. Am.*, **54** (1964b), 755-776.

ANDERSON, DON L., Recent evidence concerning the structure and composition of the earth's mantle, *Phys. Chem. Earth*, **6** (1965), 1-131.

ANDERSON, DON L., Latest information from seismic observations, Chapter 12, in *The Earth's Mantle*, edited by T.F. Gaskell, (1967), pp. 355-420, Academic Press, London.

ANDERSON, DON L., and M.N. TOKSÖZ, Surface waves on a spherical earth, 1, *J. Geophys. Res.*, **68** (1963), 3483-3500.

BACKUS, G., and F. GILBERT, The rotational splitting of the free oscillations of the earth, *Proc. Natl. Acad. Sci. U.S.*, **47** (1961), 362-371.

BÅTH, M., Lateral inhomogeneities of the upper mantle, *Tectonophysics*, **2** (1965), 483-514.

BENIOFF, H., F. PRESS, and S.W. SMITH, Excitation of the free oscillations of the earth by earthquakes, *J. Geophys. Res.*, **66** (1961), 605-619.

BLACKMAN, R.B., and J.W. TUKEY, *The Measurement of Power Spectra*, (1958), 190 pp, Dover Publ., New York.

BOLT, B.A., Recent information on the earth's interior from studies of mantle waves and eigenvibrations, *Phys. Chem. Earth*, **5** (1964), 55-119.

BULLEN, K.E., and R.A.W. HADDON, Derivation of an earth model from free oscillation data, *Proc. Natl. Acad. Sci. U.S.*, **58** (1967), 846-852.

CONNES, J., P.A. BLUM, G. JOBERT, and N. JOBERT, Observation des oscillations propres de la terre, *Ann. Geophys*, **18** (1962), 260-268.

COOLEY, J.W., and J.W. TUKEY, An algorithm for the machine calculation of complex Fourier series, *Mathematics of Computation*, **19** (1965), 297-301.

DERR, J.S., A comparison of free oscillations of oceanic and continental earth models, *Bull. Seism. Soc. Am.*, **57** (1967), 1047-1061.

DZIEWONSKI, A., and M. LANDISMAN, Great circle Rayleigh and Love wave dispersion from 100 to 900 seconds, (1969), in press.

GILBERT, F., and G. BACKUS, The rotational splitting of the free oscillations of the earth,

2, *Rev. Geophys.*, **3** (1965), 1-9.

HADDON, R. A. W., and K. E. BULLEN, An earth model incorporating free earth oscillation data, *Phys. Earth Planet. Interiors*, **2** (1969), 35-49.

HAGIWARA, T., A note on the theory of the electromagnetic seismograph, *Bull. Earthq. Res. Inst.*, **36** (1958), 139-164.

KANAMORI, H., Application of synthetic seismograms to determination of source parameters (abstract), *Trans. Am. Geophys. Union*, **50** (1969), 238, full text in preparation.

KANAMORI, H., Velocity and Q of mantle waves, *Phys. Earth Planet. Interiors*, **2** (1970), in press.

KOVACH, R. L., Seismic surface waves: Some observations and recent developments, *Phys. Chem. Earth*, **6** (1965), 251-314.

MACDONALD, G. J. F., and N. F. NESS, A study of the free oscillations of the earth, *J. Geophys. Res.*, **66** (1961), 1865-1911.

NAGAMUNE, T., Y. SATÔ, and M. SAITO, Short period free oscillation of the earth caused by the Chilean Earthquake of May 22, 1960 and related problems, *Jour. Phys. Earth*, **12** (1964), 37-41.

NESS, N. F., J. C. HARRISON, and L. B. SLICHTER, Observations of the free oscillations of the earth, *J. Geophys. Res.*, **66** (1961), 621-629.

NOWROOZI, A. A., Eigenvibrations of the earth after the Alaskan earthquake, *J. Geophys. Res.*, **70** (1965), 5145-5156.

NOWROOZI, A. A., Measurement of Q values from the free oscillations of the earth, *J. Geophys. Res.*, **73** (1968), 1407-1415.

PEKERIS, C. L., Z. ALTERMAN, and H. JAROSCH, Rotational multiplets in the spectrum of the earth, *Phys. Rev.*, **122** (1961), 1962-1700.

PRESS, F., Long-period waves and free oscillations of the earth, *Research in Geophysics*, vol. 2, edited by H. Odishaw, (1964), pp. 1-26, MIT Press, Cambridge.

PRESS, F., A. BEN-MENAHEM, and M. N. TOKSÖZ, Experimental determination of earthquake fault length and rupture velocity, *J. Geophys. Res.*, **66** (1961), 3471-3485.

SAITO, M., Excitation of free oscillations and surface waves by a point source in a vertically heterogeneous earth, *J. Geophys. Res.*, **72** (1967), 3689-3699.

SATO, R., Attenuation of seismic waves, *Jour. Phys. Earth*, **15** (1967), 32-61.

SATÔ, Y., and T. USAMI, Method of determining the degree of free oscillation of a radially heterogeneous elastic sphere, *Bull. Earthq. Res. Inst.*, **41** (1963), 331-342.

SATÔ, Y., T. USAMI, and M. LANDISMAN, Theoretical seismograms of spheroidal type on the surface of a gravitating elastic sphere. II, Case of Gutenberg-Bullen A' earth model., *Bull. Earthq. Res. Inst.*, **45** (1967), 601-624.

SATÔ, Y., T. USAMI, and M. LANDISMAN, Theoretical seismograms of torsional disturbances excited at a focus within a heterogeneous spherical earth—Case of a Gutenberg-Bullen A' earth model, *Bull. Seism. Soc. Am.*, **58** (1968), 133-170.

SMITH, S. W., An investigation of the earth's free oscillations, Ph. D. thesis, California Institute of Technology, Pasadena, (1961).

SMITH, S. W., Free oscillations excited by the Alaskan earthquake, *J. Geophys. Res.*, **71** (1966), 1183-1193.

SMITH, S. W., Free oscillation analysis and interpretation, *Trans. Am. Geophys. Union*, **48** (1967), 409-411.

STAUDER, W., and G. A. BOLLINGER, The S-wave project for focal mecanism studies, earthquakes of 1963, *Bull. Seism. Soc. Am.*, **56** (1966), 1363-1371.

TOKSÖZ, M. N., and DON L. ANDERSON, Phase velocities of long-period surface waves and structure of the upper mantle, 1. Great-circle Love and Rayleigh wave data, *J. Geophys. Res.*, **71** (1966), 1649-1658.

7. 1963年エトロフ沖地震による地球自由振動

地震研究所 阿部勝征
地震研究所 佐藤泰夫
国際地震・地震工学研究所 Jose FREZ

世界標準地震観測所のうち11ヶ所のプレス・ユーイング長周期地震計の記録をもちい，1963年10月のエトロフ沖地震の地球自由振動を解析した．自由振動の固有周期及び進行波としての位相速度，振幅の大きさ及び位相の分布に関して次の結果が得られた．

のびちぢみ振動及びねじれ振動の固有周期が周期820秒から170秒の範囲で得られた．これらの固有周期及びそれに対応する位相速度の観測値はHB1モデルの理論値に対して周期700秒付近の多少のくいちがいを除くと全体として両モードとも一致する．異なる観測点で得たそれらの値は350秒より周期の短いところで多少異なる．このことは地球の上部マントルの不均質さを示していると思われる．

のびちぢみ振動の振幅の減衰からQを求めた．平均として$Q=251$ (380～480秒)，$Q=200$ (200～380秒) である．

経度方向の分布を示すデグリーmを観測されたスペクトルとそのモードに対応する球関数の値との比較より求めた．その結果$m=0, 2$のモードが卓越し，この地震のメカニズムから推定されるものと矛盾しない．

スペクトル解析から各モードに対応する地動の平均変位を求め，それを球関数展開した．二次の項より得られた位相角N133°Eは地震断層の垂直方向を示している．

自由振動の地球表面での分布を調べるために位相の計算をした．しかし二つの観測点での位相差は予想される0ないしπにくらべてかなり不規則であつた．位相よりも振幅の大きさの方が比較的安定した結果が得られるようである．